



# A novel breast tumor classification algorithm using neutrosophic score features



Khalid M. Amin<sup>a</sup>, A.I. Shahin<sup>b</sup>, Yanhui Guo<sup>c,\*</sup>

<sup>a</sup> Department of Information Technology, Faculty of Computers and Information, Menoufiya University, Egypt

<sup>b</sup> Department of Biomedical Engineering, Higher Technological Institute, Egypt

<sup>c</sup> Department of Computer Science, University of Illinois Springfield, Springfield, IL 62703, United States

## ARTICLE INFO

### Article history:

Received 9 October 2015

Received in revised form 20 November 2015

Accepted 14 December 2015

Available online 17 December 2015

### Keywords:

Breast cancer

Ultrasound images

Feature extraction

Neutrosophic similarity score

## ABSTRACT

A lot of studies confirmed the seriousness of breast cancer as the most tumors lethal to women worldwide. Early detection and diagnosis of breast cancer are of great importance to increase treatment options and patients' survival rate. Ultrasound is one of the most frequently used methods to detect and diagnosis breast tumor due to its harmlessness and inexpensiveness. However, problems were found in the tumor diagnosis and classification as benign and malign on ultrasound image for its vagueness, such as speckle noise and low contrast. In this paper, we propose a novel breast tumor classification algorithm that combines texture and morphologic features based on neutrosophic similarity score. Then, a supervised feature selection technique is employed to reduce feature space. Finally, a support vector machine (SVM) classifier is employed to prove the discrimination power of the proposed features set. The proposed system is validated by 112 cases (58 malign, 54 benign). The experimental results show that such features set is promising and 99.1% classification accuracy is achieved.

© 2015 Elsevier Ltd. All rights reserved.

## 1. Introduction

Reports of World Health Organization (WHO) indicated that cancers are among the main reasons of morbidity and death-rate worldwide. Moreover, they reported that in 2012, the new cases are around 14 million and the cancer related deaths are 8 million [1]. For 2014, there are estimated 1.6 million new cancer cases diagnosed and 0.6 million cancer deaths only in USA [2]. Unfortunately, the total number of new cases is expected to rise – for the next two decades – by about 70% [1]. Breast cancer disease is considered the second lethal killer among women all over the world [15]. Published statistics indicate that about 8% of women will be harmed by this disease during

their lives [1]. It is believed that early detection tests for not only breast cancer but also all types of cancer save tens of thousands of lives yearly.

Breast ultrasound (BUS) imaging is a well-known approach for the early detection and diagnosis of breast cancer [3]. It is widely used in clinic due to the fact that it is noninvasive, practically harmless and low cost [4]. However, speckle noise and low contrast are their main drawbacks [5]. In addition, ultrasound exam depends on the operator's aptitude, and the analysis of its images requires good experience of the radiology field [6,7]. For more accurate diagnosis, computer-aided detection/diagnosis (CADe/CADx) systems [21–23] have been developed for detecting and classifying breast cancer. A CAD system is an interdisciplinary technology that employs both digital image processing algorithms and the knowledge of radiology's experts to greatly improve the accuracy of abnormality detection and diagnosis [8]. Generally,

\* Corresponding author.

E-mail addresses: [k.amin@ci.menofia.edu.eg](mailto:k.amin@ci.menofia.edu.eg) (K.M. Amin), [ahmed.esmail@hti.edu.eg](mailto:ahmed.esmail@hti.edu.eg) (A.I. Shahin), [yguo56@uis.edu](mailto:yguo56@uis.edu) (Y. Guo).

ultrasound CAD system includes many stages on image processing: (a) denoising, (b) enhancement, (c) segmentation, (d) feature extraction, (e) features reduction and finally (f) classification. Some simple CAD systems start processing using already segmented images [15]. In such systems, many features are extracted from the segmented region of interest. Then, this large number of features are reduced and used as inputs to the next classifier stage. Our proposed system in this work is designed according to the latter approach.

The input to our proposed system is a breast ultrasound image which contains only one tumor. The tumor's contour is marked by an experienced radiologist. The rectangular image that best enclose the tumor area (ROI) is then selected from the input image. Different types of features are extracted from the ROI image and included in a features pool. In order to reduce the size of such pool, a supervised chi-squared feature selection technique is employed. To classify the tumor into either benign or malign classes, a support vector machine classifier is used as a final stage.

The rest of this paper is organized as follows. Section 2 gives a brief review of literature. Section 3 presents the details of the proposed method. In Section 4, Experimental results are introduced and then followed by a discussion in Section 5. Finally, Conclusions and future work are drawn in Section 6.

## 2. Literature review

During the last few years, classification of breast tumors in ultrasound images is a hot research point. Many CAD systems were proposed to distinguish malignant from benign tumors in BUS images. A survey on the research work done during last few years on such CAD systems is summarized in Table 1. We are here interested in the stages of feature extraction, feature reduction/selection, and classification. Table 1 demonstrates some specific points used in similar recent CAD systems. For every previous work; the total size of used data set and the number of malignant and benign cases are indicated. The training and testing partitions of the dataset (if any) is also indicated. In such table, the employed type of classifier/or classifiers, the obtained classification accuracy, types and numbers

of extracted features, used feature reduction/selection (if any) are indicated. The used abbreviations are summarized in the last row of Table 1.

### 2.1. Features extraction

Features can generally be used as a concise representation of an image [12]. From the radiologist's point of view, while investigating BUS images, malignant tumors have many different characteristics (shape, margins, structure, texture, ...) than benign ones. The main characteristics of malignant tumors are: irregular shape, malady boundaries, microlobulated margins and heterogeneous echo texture [19]. On the other hand, benign tumors have a rounded shape, well defined margins, and homogeneous echo texture. However, the boundary and shape characteristics are the most important information in tumor's detection or differentiation [18,19].

From the digital image processing point of view, the features extracted from a BUS image are usually a combination of two or more categories of: texture, morphological, model-based, and descriptor features. A brief summary of them that were utilized in detection and classification of tumors in BUS images can be found in [15,28]. Due to the complicated nature of Model-based and descriptor features [28], we are interested here on the texture and morphologic features.

#### 2.1.1. Texture features

One of an effective and robust set of features that is used to classify breast tumors is the texture features [15]. It is clearly noted from survey results summarized in Table 1 that texture features are the most popular features that are extracted from BUS images [24–26,28,31].

In [24], nine auto-covariance coefficients were used as texture features extracted from ROI image. In [25], The ROI image is divided into non-overlapping grids, then, local texture features, local gray level co-occurrence matrix (GLCM) features and position features (to indicate the position of each grid with respect to center of ROI image) are extracted. Local texture features include different measures that quantitatively describe the first order histogram of each grid [25].

**Table 1**  
Survey of recent CAD systems [24–32].

References	Size of data-set	Classifier	Accuracy (%)	Features (Total No.)	Feature reduction
[24]	210 (120 B, 90 M)	SVM	93	Text. & Morph. (T: 9)	Fwd. F/S
[25]	132 (67 B, 65 M)	APC	93	Text. & Morph. (T: 9)	PCA, SFSS
[26]	105 (50 B, 55 M)	SVM	94	Text. & Morph. & Vascularity (T: 9)	No
[27]	200 (100 M, 100B)	SVM Ada.	95 93	Text. (shearlet trnsf.) (NA)	No
[28]	321 (92 B, 172 M) {train} (21 B, 36 M) {test}	SVM ANN KNN	87 87 84	Text. & Morph. (T: 140)	No
[29]	80 (47 B, 33 M)	SVM	87	Text. & Morph. (T: 6)	No
[30]	40	SVM	93	Text. & Morph. (T: 9)	PCA 2D-LDA
[31]	91 (56 B, 35 M)	ANN	98	Text. (T: 300)	Fischer algorithm
[32]	80 (21B, 59 M)	Multi-C (ANN& Ada.& FSVM)	99	Text. (37)& Morph.(20)	Bidirectional search

Used Abbreviations; T: Total No. of features, F/S: feature selection, Text.: Texture, Morph.: Morphologic, APC: Affinity propagation clustering, Trnsf.: transform, Multi-C: multi classifier, Ada.: Ada-boost, SFSS: Sequential floating forward selection.

A histogram of an image is a function indicating the number of pixels that have the same intensity level [14]. For an gray image  $f$  with size  $(N \times M)$ , Let  $(f(x,y) = i)$  be a function of two variables  $x$  (horizontal space variable) and  $y$  (vertical space variable), where  $x = 0, 1, \dots, N-1$  and  $y = 0, 1, \dots, M-1$ . Let  $G$  represents the number of intensity levels in  $f$ , then the discrete value ( $i$ ) of function  $f(x,y)$  equals  $i = 0, 1, \dots, G-1$ . The intensity-level histogram is given as [9]:

$$h(i) = \sum_{x=0}^{N-1} \sum_{y=0}^{M-1} \delta(f(x,y), i) \quad (1)$$

where  $\delta(j, i)$  represents Kronecker delta function which is defined by;

$$\delta(j, i) = \begin{cases} 1 & \dots j = i \\ 0 & \dots j \neq i \end{cases} \quad (2)$$

The pdf of occurrence of intensity levels is obtained by dividing  $h(i)$  by  $(N \times M)$  which indicates the total number of pixels [9]:

$$P(i) = \frac{h(i)}{N \cdot M}, \quad i = 0, 1, \dots, G-1 \quad (3)$$

The following four basic statistical measures can be used as texture features [35] and calculated for each image histogram using [9]:

$$\text{Mean: } \mu = \sum_{i=0}^{G-1} i p(i) \quad (4)$$

$$\text{Variance: } \sigma^2 = \sum_{i=0}^{G-1} (i - \mu)^2 p(i) \quad (5)$$

$$\text{Skewness: } \mu^3 = \sigma^{-3} \sum_{i=0}^{G-1} (i - \mu)^3 p(i) \quad (6)$$

$$\text{Kurtosis: } \mu^4 = \sigma^{-4} \sum_{i=0}^{G-1} (i - \mu)^4 p(i) - 3 \quad (7)$$

GLCM is another method to describe the textures by considering the spatial relationship of the pixels on images [25,26]. For a given image, the GLCM is calculated by counting how many times- pairs of pixels with specific values and relative direction- are found. Hence, some statistical measures can be calculated from this matrix and used as texture features. By definition, the number of gray levels in the image  $G$  determines and equals the number of either rows or columns of the GLCM which is a square matrix [10]. In the calculated GLCM, each element  $C(i, j, d, \theta)$  is the sum of the number of times that the pixel with value  $i$  occurred in the specified spatial relationship to a pixel with value  $j$  in the input image. The spatial relationship is specified by the distance  $d$  (1, 2, 3, ...) between the pair of pixels along direction angle  $\theta$  ( $0^\circ, 45^\circ, 90^\circ, \text{ or } 135^\circ$ ) of the image [26]:

$$C_{(d,\theta)}(i,j,d,\theta) = \|\{(x_1,y_1), (x_2,y_2) | x_2 - x_1 = d \cos \theta, y_2 - y_1 = d \sin \theta, I(x_1,y_1) = i, I(x_2,y_2) = j\}\| \quad (8)$$

where  $(x_1, y_1)$  and  $(x_2, y_2)$  are the pixels in the ROI,  $I(\cdot)$  is the intensity, and  $\|\cdot\|$  is the number of pixel pairs matching to the specified conditions [26].

In [2,3,5], many typical statistical features can be extracted from GLCM at different  $(G, d, \theta)$  values. In the work of [27], texture features are extracted based on shear-let transform. In a recent work of [31], 300 texture features are extracted based on the histogram, absolute gradient (spatial variation of gray-level values), run length matrix (counts of pixel runs with the specified gray-level value and length in a given direction), GLCM, autoregressive model (description of correlation between neighboring pixels), and wavelet (decomposition image frequency at different scales).

### 2.1.2. Morphologic (shape) features

Most CAD systems [24–26,28–30,32] used morphologic features to cooperate with texture features in order to achieve higher classification accuracy. Morphologic features are used to describe shape and margin of the tumors [15]. The shape is an effective feature for classifying breast tumors into benign and malignant [19]. Some popular morphological features of interest are defined as follows [11–13]:

- **Diameter ( $di$ ):** It is a feature of any component that has area and perimeter. The diameter feature represents here the diameter of the tumor. It can be calculated as an average length of the axis in irregular shapes.
- **Eccentricity ( $ec$ ):** It is defined by the ratio of the distance between the foci of the ellipse and its major axis length. It takes values between 0 and 1. As an example, for an ellipse that has zero  $ec$ , it is actually a circle. Moreover, for an ellipse whose  $ec$  is 1, it is a segment of straight line.
- **Perimeter ( $pr$ ):** It represents the total length of the component perimeter. Since malignant tumors usually have irregular shapes, large value of  $pr$  is associated with that a tumor is probably malignant.
- **Area ( $ar$ ):** Malignant tumors usually have a larger value of  $ar$  compared to benign tumors.
- **Circularity ( $cr$ ):** It's a measure of the compactness of a shape. For an example, a circle is the most compact and round shape. Benign tumors have usually larger circularity than malignant ones. The  $cr$  is calculated by;

$$cr = \frac{4 \times \pi \times ar}{(pr)^2} \quad (9)$$

- **Elongation ( $el$ ):** the ratio between the object's longest axis ( $lx$ ) and its shortest axis ( $sx$ ). Malignant tumors have usually larger elongation than benign ones. Shape elongation is calculated using;

$$el = \frac{sx}{lx} \quad (10)$$

- **Compactness ( $co$ ):** This feature depends on circularity and elongation as following;

$$co = cr \times el \quad (11)$$

## 2.2. Features selection

A lot of features can be extracted from BUS images. It is not an ideal option to employ all features for classification, and the selection of optimal and relevant features is crucial for accurate classification decision [15,17]. The required training time and classification accuracy are greatly affected by the dimension of features vector [15]. In the literature, many feature reduction/selection techniques were used such as: principal component analysis (PCA) [25], forward feature selection [24], sequential floating forward selection (SFFS) [3], bidirectional search [32], Fischer algorithm [31], linear discriminate analysis (LDA) [30].

## 2.3. Classification

The following block after the features reduction is the classifier which uses the reduced features pool to categorize the tumor in an BUS image into benign/malignant [15]. In the literature, many types of classifiers were used. Our survey summary in Table 1 illustrates that SVM, due to its superior performance and time cost [15], is the most popular classifier used by recent CAD systems as in [24,26–30]. Artificial neural network (ANN) (with different topologies) and ada-boost are also used for comparison reasons as in [28]. Sometimes, many classifiers are combined in the same system and a majority voting method was used to get the final result [30].

For the scheme of training and testing, some systems (e.g. in [28]) divided the images dataset into training and testing sections. Others utilized *x*-cross folding techniques.

For the evaluation of the classification results, unfortunately, according to our knowledge, there is no standard BUS image database available to be used as a benchmark [15]. Most of the previous work, as also noted from Table 1, were done by using their own databases, which are of different sizes, portions of benign and malignant classes, and sources. Different metrics are used for measuring performance such as [15,24–32]: a receiver operating characteristic (ROC) curve, overall accuracy (ACC), specificity (SPC), sensitivity or true positive rate (TPR), precision or positive predictive value (PPV), negative predictive value (NPV).

## 2.4. Neutrosophic similarity score

The neutrosophic similarity score (NSS) algorithm is relatively new and introduced by [33] to measure the degree to the ideal object, and it has been applied widely due to its ability to describe the indeterminate features. A neutrosophic set can be defined under different criteria as: let  $A = \{A_1, A_2, \dots, A_m\}$  be a set of alternatives in neutrosophic set, and  $C = \{C_1, C_2, \dots, C_n\}$  be a set of criteria. The alternative  $A_i$  at  $C_j$  criterion is denoted as  $\{T_{C_j}(A_i), I_{C_j}(A_i), F_{C_j}(A_i)\}/A_i$ , where  $T_{C_j}(A_i)$ ,  $I_{C_j}(A_i)$  and  $F_{C_j}(A_i)$  are the membership values to the true, indeterminate and false set at the  $C_j$  criterion.

A similarity score is employed to measure the similarity between two elements in neutrosophic set under multi-criteria [33]:

$$S_{C_j}(A_m, A_n) = \frac{T_{C_j}(A_m)T_{C_j}(A_n) + I_{C_j}(A_m)I_{C_j}(A_n) + F_{C_j}(A_m)F_{C_j}(A_n)}{\sqrt{T_{C_j}^2(A_m) + I_{C_j}^2(A_m) + F_{C_j}^2(A_m)}\sqrt{T_{C_j}^2(A_n) + I_{C_j}^2(A_n) + F_{C_j}^2(A_n)}} \quad (12)$$

The concept of ideal element can be employed to identify the best alternative. The ideal alternative  $A^*$  is denoted as:  $\{T_{C_j}^*(A_i), I_{C_j}^*(A_i), F_{C_j}^*(A_i)\}/A_i^*$ . The similarity to the ideal alternative is calculated as:

$$S_{C_j}(A_i, A^*) = \frac{T_{C_j}(A_i)T_{C_j}(A^*) + I_{C_j}(A_i)I_{C_j}(A^*) + F_{C_j}(A_i)F_{C_j}(A^*)}{\sqrt{T_{C_j}^2(A_i) + I_{C_j}^2(A_i) + F_{C_j}^2(A_i)}\sqrt{T_{C_j}^2(A^*) + I_{C_j}^2(A^*) + F_{C_j}^2(A^*)}} \quad (13)$$

$U$  is a universe,  $BP$  is a bright pixel set in  $U$ , and an image  $I_m$  in NS domain is named as neutrosophic image  $I_{NS}$ , which is interpreted using subsets  $T$ ,  $I$  and  $F$ . A pixel  $P(x, y)$  is interpreted in NS domain:  $P_{NS}(x, y) = \{T(x, y), I(x, y), F(x, y)\}$ .  $T(x, y)$ ,  $I(x, y)$  and  $F(x, y)$  are memberships belonging to bright pixel set, indeterminate set and non-bright pixel set, respectively. At the intensity criterion, they are computed as:

$$T_{C_g}(x, y) = \frac{g(x, y) - g_{\min}}{g_{\max} - g_{\min}} \quad (14)$$

$$I_{C_g}(x, y) = 1 - \frac{Gd(i, j) - Gd_{\min}}{Gd_{\max} - Gd_{\min}} \quad (15)$$

$$F_{C_g}(x, y) = 1 - T_{C_g}(x, y) \quad (16)$$

where  $g(x, y)$  and  $Gd(x, y)$  are the gray scale value and gradient magnitude value at the position of  $(x, y)$  on the image. Finally, to measure the degree to the ideal object under intensity condition, a similarity score is calculated using:

$$S_{C_g}(P(x, y), A^*) = \frac{T_{C_g}(x, y)T_{C_g}(A^*) + I_{C_g}(x, y)I_{C_g}(A^*) + F_{C_g}(x, y)F_{C_g}(A^*)}{\sqrt{T_{C_g}^2(x, y) + I_{C_g}^2(x, y) + F_{C_g}^2(x, y)}\sqrt{T_{C_g}^2(A^*) + I_{C_g}^2(A^*) + F_{C_g}^2(A^*)}} \quad (17)$$

## 3. Proposed method

This section discusses our brief CAD system which starts processing not from raw BUS images, but from segmented ones. The proposed method of classifying BUS images is comprised of the following four fundamental stages:

- *Region of interest (ROI) selection:* ROI image which only includes the tumor region is selected from the original BUS image according to markings of the radiologist.
- *Feature extraction:* different types of information are extracted from ROI image. This extracted information is used to create a feature pool. Our proposed features are extracted based on NSS domain.
- *Feature selection:* Supervised chi-squared feature selection technique is used to reduce the size of features pool.
- *Classification:* In the last phase, we use support vector machine (SVM) classifier to give us the final classification decision.

These four stages are described in more detail in the following sub-sections along with the steps involved. The flow chart in Fig. 1 illustrates the detailed steps of our proposed method. All original marked BUS images are available in RGB format. The input BUS image is converted into gray level image (from which texture features are extracted) and then into binary image (from which shape features are extracted) as two preliminaries steps. Then, the ROI is selected and partitioned into nine sub-images so as to be ready for feature extraction stage. The same partitioning technique is also applied to the ROI image after being transformed to the NS domain. The details of creation of different features vectors and pools are discussed later. A classifier is used as a final stage to give the decision: malign or benign tumor.

### 3.1. ROI selection and partition

In a BUS image, a ROI is a rectangle enclosing the lesion. Hence, the rectangle ROI image may have minor areas of surrounding tissues that may lead to minor errors in the experimental results. An illustrative example of ROI selection and partitioning is shown in Fig. 2. An original BUS image, that has only one tumor, is shown in Fig. 2a. The

tumor on image is marked by an experienced radiologist as shown in Fig. 2b, and selection of ROI is illustrated in Fig. 2c.

For measuring the feature distribution in different sub-regions inside ROI, a method is newly proposed to split the ROI into several sub-images with equal areas as shown in Fig. 2d based on the fact that the center of the tumor has different feature distribution from the boundary parts. According to such splitting technique, every sub-region is called “SRx”, where x equals (1, 2, ... or 9). Usually, “SR5” represents the tumor centered region. Moreover, all other sub-images represent different contour parts of the tumor. The partitioned BUS image of Fig. 2a is shown in Fig. 2e. This method is useful to describe various regions of the tumor and is ready now for following feature extraction stage.

### 3.2. Feature extraction

In this section, we employ both texture and morphological features to describe the tumor in each ROI image. These traditional features are combined together into a single features pool (FP1) which is consisting of 85 features described in the following subsections in detail. Moreover,

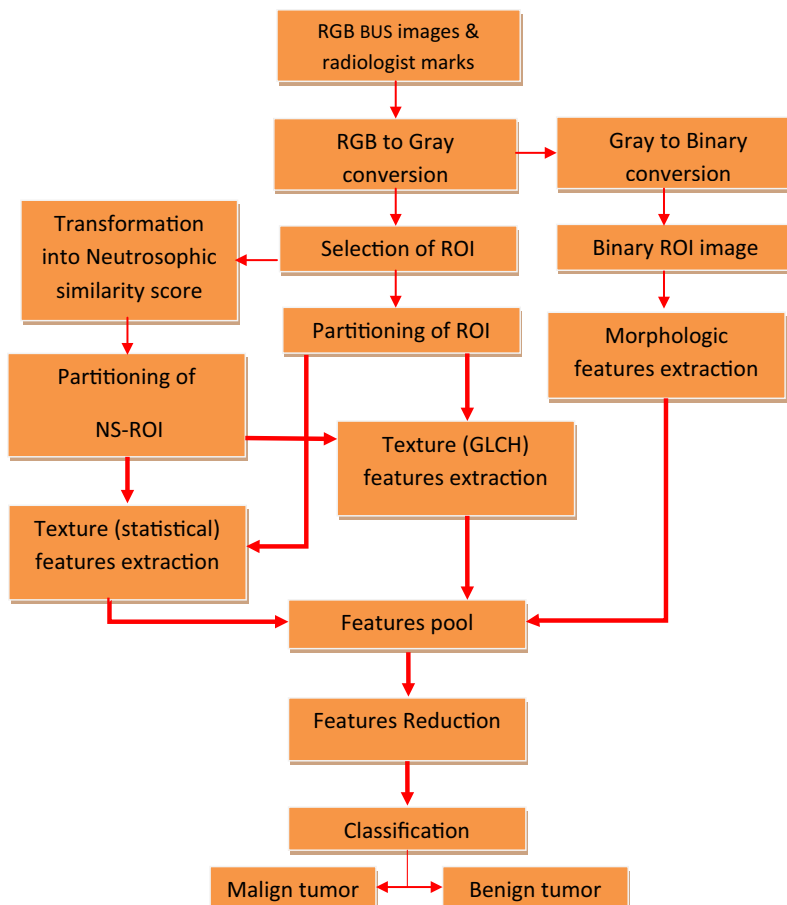
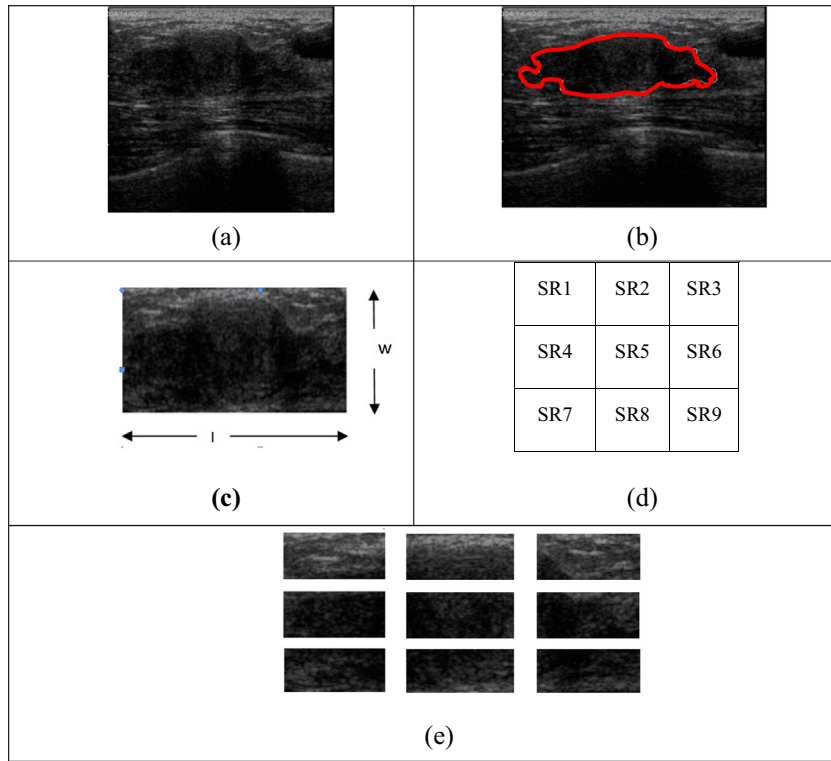


Fig. 1. Flow chart of the proposed method.



**Fig. 2.** Processing stages of an BUS as an example; (a) a raw BUS image, (b) Marked BUS image, (c) Selected ROI (with dimensions  $l \times w$ ), (d) partitioning of ROI image into equaled area nine sub-regions. The length of each sub-region is  $(l/3)$ , width is  $(w/3)$  (e) Partitioned ROI image.

we propose a novel feature pool (FP2) which is extracted from the transformed ROI image in the neutrosophic set domain and using the neutrosophic similarity score.

3.2.1. Intensity based features

For each sub-image in the partitioned ROI image (as shown in Fig. 3d), the basic four statistical features (F1: mean, F2: variance, F3: skewness, F4: kurtosis) of intensity histogram are extracted. Then, the resultant features that are extracted from the entire image are 36 features. The

following novel features are proposed to measure horizontal, vertical and central orientation contrast of intensity. Such features are calculated depending on the above 36 features extracted:

F5: Horizontal orientation contrast of intensity (CH)

$$CH = \frac{|F1_{SR2} + F1_{SR5} + F1_{SR8} - \frac{1}{2}(F1_{SR1} + F1_{SR4} + F1_{SR7} + F1_{SR3} + F1_{SR6} + F1_{SR9})|}{F1_{SR2} + F1_{SR5} + F1_{SR8}} \quad (18)$$

F6: Vertical orientation contrast of intensity (IVH)

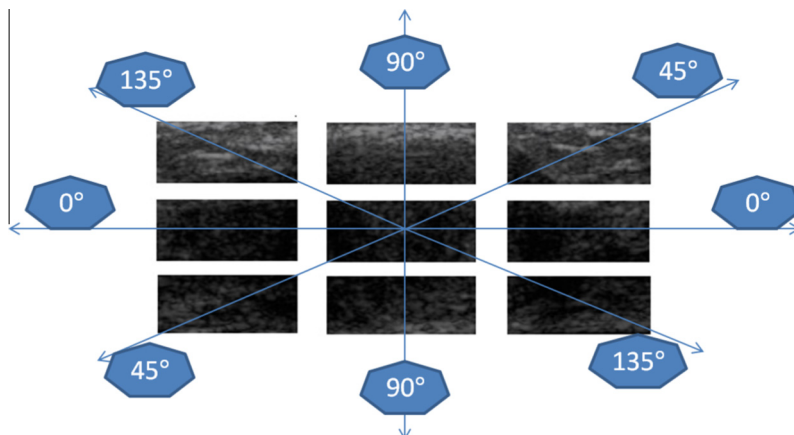


**Fig. 3.** The most important direction of variation for each sub-image is indicated on different axis.

$$IVH = \frac{|F1_{SR4} + F1_{SR5} + F1_{SR6} - \frac{1}{2}(F1_{SR1} + F1_{SR2} + F1_{SR3} + F1_{SR7} + F1_{SR8} + F1_{SR9})|}{F1_{SR4} + F1_{SR5} + F1_{SR6}} \quad (19)$$

F7: Central contrast of intensity (ICC)

$$ICC = \frac{|F1_{SR5} - \frac{1}{8}(F1_{SR1} + F1_{SR2} + F1_{SR3} + F1_{SR4} + F1_{SR6} + F1_{SR7} + F1_{SR8} + F1_{SR9})|}{F1_{SR5}} \quad (20)$$

Hence, the first features vector will be called “FV1” and includes 39 features (36 features, F5, F6, and F7). Such feature vector represents the basic intensity-based statistical features of the ROI image.

### 3.2.2. Texture (GLCM-based) features

From the above literature review, the intensity-based features should be enforced with other types of texture features. As a second texture descriptor, a gray level co-occurrence histogram (GLCH) is calculated from the GLCM of each sub-image with parameters values that are listed in Table 2. The value of angle  $\theta$  is selected for each sub-image to indicate the most important direction of variation in the tumor texture as shown in Fig. 2. For  $0^\circ$  axis, the horizontal direction is the most important direction of variation, so,  $\theta$  is selected to be zero for SR4, SR5 and SR6. Also, For  $45^\circ$  axis,  $\theta$  is selected to be  $45^\circ$  for SR3 and SR7, and so on. We then, extract the four basic statistical features {F8  $\equiv$  Mean, F9  $\equiv$  Variance, F10  $\equiv$  Skewness, F11  $\equiv$  Kurtosis} from GLCH on each sub-image. As a result, 36 features are extracted from the entire image. Moreover, extra novel features which are calculated based on the above features as defined as follows;

F12: Horizontal orientation contrast of texture (TCH):

$$TCH = \frac{|F8_{SR2} + F8_{SR5} + F8_{SR8} - 0.5(F8_{SR1} + F8_{SR4} + F8_{SR7} + F8_{SR3} + F8_{SR6} + F8_{SR9})|}{F8_{SR2} + F8_{SR5} + F8_{SR8}} \quad (21)$$

F13: Vertical orientation contrast of texture (TVC):

$$TVC = \frac{|F8_{SR4} + F8_{SR5} + F8_{SR6} - 0.5(F8_{SR1} + F8_{SR4} + F8_{SR7} + F8_{SR3} + F8_{SR6} + F8_{SR9})|}{F8_{SR4} + F8_{SR5} + F8_{SR6}} \quad (22)$$

F14: Central contrast of texture (TCC):

$$TCC = \frac{|F8_{SR5} - 0.125(F8_{SR1} + F8_{SR2} + F8_{SR3} + F8_{SR4} + F8_{SR6} + F8_{SR7} + F8_{SR8} + F8_{SR9})|}{F8_{SR5}} \quad (23)$$

The above GLCH features are concatenated into the feature vector which will be called “FV2” and includes 39 features.

### 3.2.3. Morphologic features

For nearly all of previous CAD systems, morphologic features are used to coincide with texture features so as to get maximum classification accuracy. Here in our proposed system, we use some morphologic features to describe the shape of the tumor’s contour. The contour shape of either benign or malignant tumors can be described by the following features that are included in the feature vector “FV3” that includes seven features; F15: Diameter, F16: Eccentricity, F17: Perimeter, F18: Area, F19: Circularity, F20: Elongation, F21: Compactness.

**Table 2**

Detailed values of different parameters of GLCM.

Parameter	Value
Number of gray levels, $G$	8
Distance between pixels, $d$	1
Direction of variation, $\theta$	Depends on the location in the ROI
	SR1, $135^\circ$ SR2, $90^\circ$ SR3, $45^\circ$
	SR4, $0^\circ$ SR5, $0^\circ$ SR6, $0^\circ$
	SR7, $45^\circ$ SR8, $90^\circ$ SR9, $135^\circ$

**Table 3**

List of used abbreviations for various features vectors.

Abbrev.	Features	No. of elements
FV1	1st order statistical	39
FV2	GLCH	39
FV3	Morphological	7
FV4	{FV1, FV2}	78
FV5	{FV1, FV3}	46
FV6	{FV2, FV3}	46
FP1	{FV1, FV2, FV3}	85
FP2	{FV1 <sub>NS</sub> , FV2 <sub>NS</sub> , FV3 <sub>NS</sub> }	85

### 3.2.4. Features pool

To reveal the discriminative power of various types of features, the following concatenated vectors are proposed; FV4 = {FV1, FV2}, FV5 = {FV1, FV3}, FV6 = {FV2, FV3}. Finally, the above feature vectors FV1, FV2 and FV3 are concatenated all together to construct the features pool “FP1”. On the other hand, all ROI images are transformed to the neutrosophic domain “ROI\_NS” which from the various novel feature vectors (FV1<sub>NS</sub>, FV2<sub>NS</sub>, FV3<sub>NS</sub>) are extracted to construct the feature pool “FP2”. Table 3 lists the abbreviations used for various features vectors.

### 3.3. Feature selection

The proposed features pool consists of 85 features. The dimension of feature vectors should be reduced to enhance the performance of the classifier, and to shorten the training time of the algorithm [15]. In our work, we use the Chi\_squared ( $\chi^2$ ) feature selection technique which gives promised results in a recent similar work [17].

### 3.4. Classification

In our proposed system, we use support vector machine (SVM) for it is an effective statistical learning method for classification [16]. SVM also has advantage of fast training technique, even with large number of input data. Therefore, it has been used for many pattern classification problems [20]. We use the most popular 10-folds cross validation method for dividing the dataset into training and testing data.

## 4. Experimental results

### 4.1. BUS images database

A clinical BUS images database [8] is used in the experiments. The images were collected by an experienced radiologist in the 2nd Affiliated Hospital of Harbin Medical

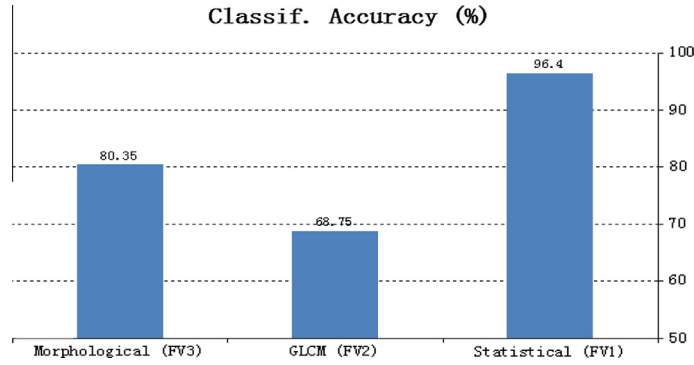


Fig. 4. Comparison between classification accuracies using different features types. Only one feature vector is used per experiment.

University, Harbin, China. The used equipment: VIVID 7 (GE, USA) with a 5–14 MHz linear probe, and captured directly from video frames. The database includes one BUS image for 112 cases where each image contains only a single lesion. The 112 images include 54 cases for benign solid lesions, and 58 cases for malignant solid lesions. All cases were confirmed by either biopsy or operation. Finally, experienced radiologists outlined tumors in each BUS image. Such marked images are used as golden standard images [8]. During our experiments, we use both Matlab (release 2014a) [34] and Weka (Ver. 3.6.11) [35] as software tools.

4.2. Performance metrics

Different metrics are used to measure the performance of the classification process. On the basis of the obtained confusion matrix, we can define: TP ≡ True positive, TN ≡ True negative, FP ≡ False positive, FN ≡ False negative. Then, five metrics can be calculated as follows [13];

$$Accuracy = \frac{TP + TN}{TP + TN + FP + FN} \tag{24}$$

$$Sensitivity = \frac{TP}{TP + FN} \tag{25}$$

$$Specificity = \frac{TN}{TN + FP} \tag{26}$$

$$Positive\ predictive\ value\ (PPV) = \frac{TP}{TP + FP} \tag{27}$$

$$Negative\ predictive\ value\ (NPV) = \frac{TN}{TN + FN} \tag{28}$$

4.3. Features discriminability test

In the first experiment, we show the discriminability of various features. In a three successive classification experiments using the SVM classifier, the features vector (FV1, FV2, or FV3) is used to train and test the classifier using 10-folds cross validation technique. Fig. 4 illustrates the classification accuracy for each features vector. FV1 gives the maximum classification accuracy (96.4%). When FV2 only is used. It gives accuracy of 68.75%. Moreover, FV3 gives (80.35%) classification accuracy.

4.4. Combined features discriminability test

In the second experiment, we want to show that combinations of the above feature vectors gives higher accuracy than using each one individually. Using the same setup described in the above first experiment, Fig. 5 illustrates a comparison between the classification accuracy obtained when using the features vector (FV4, FV5 or FP1).

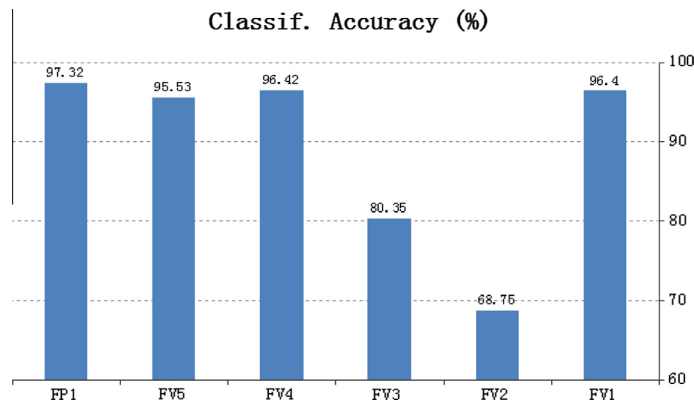


Fig. 5. Classification accuracy for combined features.

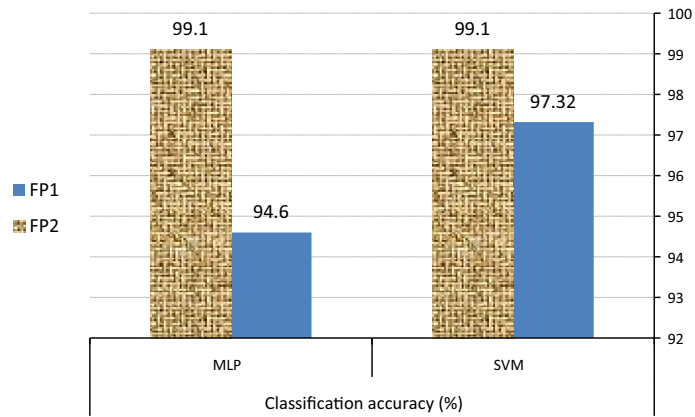


Fig. 6. Comparison between the classification accuracy of SVM and MLP for FP1 and FP2.

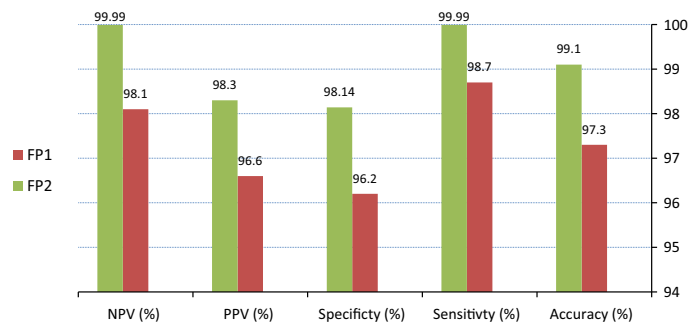


Fig. 7. Calculated different performance metrics for the classification using features pool (FP1) and neutrosophic features pool (FP2).

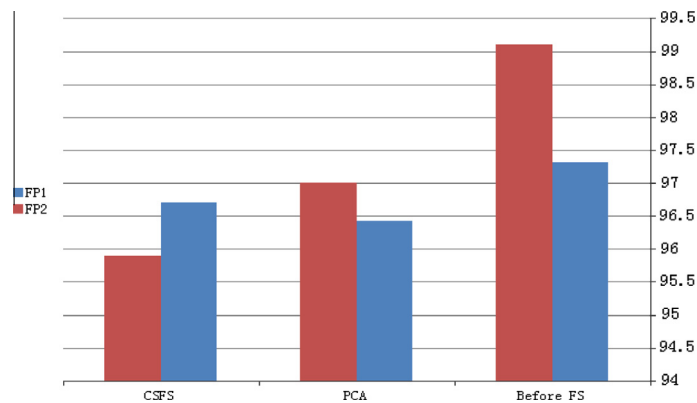


Fig. 8. classification accuracy for both (FP1 and FP2) after features dimension reduction using CSFS and PCA.

4.5. performance of our novel features

In the third experiment, we compare between the classification accuracy using our proposed novel features pool (FP2) and traditional features pool (FP1). As shown in Fig. 6, FP2 gives better performance (99.1%) than that of FP1 (97.32%). A comparison between the accuracy of SVM and another common neural network classifier (Multi layer Perceptron “MLP”) for both FP1 and FP2 is shown also in Fig. 6. As stated above in the literature review section, SVM gives better performance. Different performance

metrics (accuracy, sensitivity, specificity, PPV, NPV) are calculated for both FP1 and FP2 as shown in Fig. 7. For all measures, SVM is used to classify different pools without using any dimension reduction techniques. It is obvious the using of FP2 gives super classification performance in all metrics.

4.6. Performance of feature reduction technique

In order to reduce the size of the feature vector, we used the Chi-squared feature selection (CSFS). For comparison

purposes, we use also the popular feature reduction technique; principal component analysis (PCA). Fig. 8 shows comparison between such methods for FP1.

## 5. Discussion

As a primary test, we check the discrimination power of every type of the used features both when it is used separately and when multiples of them are used together. Employing of only FV1, FV2, or FV3 gives classification accuracy 96.4%, 68.7% and 80.3% respectively. This means that FV1 has the maximum discrimination power when it is used separately. In order to get higher accuracy we check all possibilities of grouping different features vectors together. When FV1 is combined with FV2 to create a new feature vector called “FV4”, they reinforce each other and give more accuracy (96.42%). When FV1 is combined with FV3 to create a new feature vector called “FV5”, they weaken each other and give lower accuracy (95.53%). When all types of features are combined together into a new feature pool called “FP1”, a classification accuracy of about (97.32%) is obtained. The latter results proved that “FP1” represents the best choice and can be used efficiently in our CAD system.

Our new proposed features pool that is called “FP2” is tested with respect to the above traditional group of features “FP1”. In our experimental results, “FP2” outperforms “FP1” with extra 1.78% classification accuracy and this is considered our main contribution in this paper. The super performance of “FP2” is clear using not only classification accuracy but also other performance metrics (e.g. sensitivity, specificity, PPV, NPV).

As expected from the results of past studies, the support vector machine (SVM) classifier gives better performance than multi layer perceptron classifier (MLP).

The effect of using of features reduction techniques is also studied. We used two famous feature reduction techniques: chi-squared features selection “CSFS” and principle component analysis “PCA”. Although the elements of the feature pool “FP1” are reduced from 85 down to 14 (using PCA) or to 5 (using CSFS) elements, classification accuracy is not greatly reduced. Moreover, computing time is greatly reduced from 6.5 s down to 0.6 s when using CSFS method.

## 6. Conclusion and future work

This paper presented a new feature extraction approach used for classifying tumors in BUS images. It combines the discriminating power of statistical and morphological features. Moreover, original BUS images are transformed into neutrosophic set domain, and then we extract the same set of features from that transformed image. That latter feature pool gives very promising classification accuracy as verified by our experiments. The dimension of features pool is greatly reduced used using chi-squared feature selection technique. We use SVM as a main classifier, and MLP-NN classifier for performance comparison. The experimental results obtained, show that classification accuracy offered by using our proposed novel features is higher than any published results. Future work will focus on optimize

the significant types of features and being tested on larger size of images database.

## Acknowledgement

The author would like to thank the second affiliated hospital of Harbin Medical University, China for providing the public breast ultrasound image dataset.

## References

- [1] <http://www.who.int/mediacentre/factsheets/fs297/en/> (accessed: 29/4/2015, 10 AM).
- [2] <http://www.cancer.org/research/cancerfactsstatistics/cancerfactsfigures2014/> (accessed 12/5/2015 10 PM).
- [3] B. Liu, H.D. Cheng, J. Huang, J. Tian, X. Tang, J. Liu, Fully automatic and segmentation-robust classification of breast tumors based on local texture analysis of ultrasound images, *Pattern Recog.* 43 (1) (2010) 280–298.
- [4] J. Shan, H.D. Cheng, Y. Wang, Completely automated segmentation approach for breast ultrasound images using multiple-domain features, *Ultrasound Med. Biol.* 38 (2) (2012) 262–275.
- [5] A. Jalalian, S.B. Mashohor, H.R. Mahmud, M.I.B. Saripan, A.R.B. Ramli, B. Karasfi, Computer-aided detection/diagnosis of breast cancer in mammography and ultrasound: a review, *Clin. Imag.* 37 (3) (2013) 420–426.
- [6] B. Sahiner et al., Malignant and benign breast masses on 3D US volumetric images: effect of computer-aided diagnosis on radiologist accuracy, *Radiology* 242 (3) (2007) 716–724.
- [7] C.M. Chen et al., Breast lesions on sonograms: computer-aided diagnosis with nearly setting-independent features and artificial neural networks, *Radiology* 226 (2) (2003) 504–514.
- [8] Yanhui Guo, Computer-aided detection of breast cancer using ultrasound images, Ph. D. thesis, Utah st. university, USA, 2010.
- [9] A. Materka, M. Strzelecki, Texture analysis methods—a review. Technical university of lodz, institute of electronics, COST B11 report, Brussels, 1998, pp. 9–11.
- [10] N. Zulpe, V. Pawar, GLCM textural features for brain tumor classification, *IJCSI Int. J. Comput. Sci. Issues* 9 (3) (2012) 354–359.
- [11] Y.L. Huang, D.R. Chen, Y.R. Jiang, S.J. Kuo, H.K. Wu, W.K. Moon, Computer aided diagnosis using morphological features for classifying breast lesions on ultrasound, *Ultrasound Obstet. Gynecol.* 32 (4) (2008) 565–572.
- [12] O. Shahin, H. Kelash, G. Attiya, O. Farag Allah, Breast cancer detection based on dynamic template matching, *Wulfenia J.* 20 (12) (2013) 193–205.
- [13] Y. Su, Y. Wang, J. Jiao, Y. Guo, Automatic detection and classification of breast tumors in ultrasonic images using texture and morphological features, *Open Med. Inform. J. (suppl. 1–M3)* (2011) 26–37.
- [14] N. Just, Improving tumour heterogeneity MRI assessment with histograms, *B. J. Cancer* 111 (2014) 2205–2213.
- [15] H.D. Cheng, J. Shan, W. Ju, Y. Guo, L. Zhang, Automated breast cancer detection and classification using ultrasound images: a survey, *Pattern Recog.* 43 (1) (2010) 299–317.
- [16] A. Mert, N. Kılıç, E. Bilgili, A. Akan, Breast cancer detection with reduced feature set, *Comput. Math. Meth. Med.* 2015 (2015). 11 pages 265138.
- [17] K. Verma, B.K. Singh, P. Tripathi, A.S. Thoke, Review of Feature Selection Algorithms for Breast Cancer Ultrasound Image, in: *New Trends in Intelligent Information and Database Systems*, Springer International Publishing, 2015, pp. 23–32.
- [18] N. Pérez, M.A. Guevara, A. Silva, Evaluation of features selection methods for breast cancer classification, in: *Icem15: 15th International Conference on Experimental Mechanics*, 2012, p. 10.
- [19] H.B. Kekre, P. Shrinath, Tumor delineation using statistical properties of the breast US images and vector quantization based clustering algorithms, *Int. J. Image, Graph. Signal Process. (IJGSP)* 5 (11) (2013) 1–12.
- [20] A.E. Hassanien, T.H. Kim, Breast cancer MRI diagnosis approach using support vector machine and pulse coupled neural networks, *J. Appl. Logic* 10 (4) (2012) 277–284.
- [21] S. Selvan, S. Shenbagadevi, S. Suresh, Computer-aided diagnosis of breast elastography and B-mode ultrasound, in: *Artif Intelligence*

- and Evolutionary Algorithms in Engineering Systems, Springer, pp. 213–223.
- [22] C.M. Lin, Y.L. Hou, T.Y. Chen, K.H. Chen, Breast nodules computer-aided diagnostic system design using fuzzy cerebellar model neural networks, *Fuzzy Syst., IEEE Trans.* 22 (3) (2014) 693–699.
- [23] K. Doi, Current status and future potential of computer-aided diagnosis in medical imaging, *Brit. J. Radiol.* (2014).
- [24] W.J. Wu, W.K. Moon, Ultrasound breast tumor image computer-aided diagnosis with texture and morphological features, *Acad. Radiol.* 15 (7) (2008) 873–880.
- [25] Y. Su, Y. Wang, J. Jiao, Y. Guo, Suppl 1: automatic detection and classification of breast tumors in ultrasonic images using texture and morphological features, *Open Med. Inform. J.* 5 (2011) 26.
- [26] Y. Liu, H.D. Cheng, J.H. Huang, Y.T. Zhang, X.L. Tang, J.W. Tian, Y. Wang, Computer aided diagnosis system for breast cancer based on color Doppler flow imaging, *J. Med. Syst.* 36 (6) (2012) 3975–3982.
- [27] S. Zhou, J. Shi, J. Zhu, Y. Cai, R. Wang, Shearlet-based texture feature extraction for classification of breast tumor in ultrasound image, *Biomed. Signal Process. Contr.* 8 (6) (2013) 688–696.
- [28] R. Liao, T. Wan, Z. Qin, Classification of benign and malignant breast tumors in ultrasound images based on multiple sonographic and textural features, in: *International IEEE Conference on Intelligent Human-Machine Systems and Cybernetics (IHMSC)*, Vol. 1, 2011, pp. 71–74.
- [29] F.S. Zakeri, H. Behnam, N. Ahmadinejad, Classification of benign and malignant breast masses based on shape and texture features in sonography images, *J. Med. Syst.* 36 (3) (2012) 1621–1627.
- [30] M.H. Yap, E.A. Edirisinghe, H.E. Bez, A comparative study in ultrasound breast imaging classification, in: *SPIE Medical Imaging*, International Society for Optics and Photonics, 2009, pp. 72591S–72591S.
- [31] A.A. Ardakani, A. Gharbali, A. Mohammadi, Classification of breast tumors using sonographic texture analysis, *J. Ultrasound Med.* 34 (2) (2015) 225–231.
- [32] B. Karimi, An automatic system for classification of breast cancer lesions in ultrasound images (Doctoral dissertation, Concordia University), 2014.
- [33] Y. Guo, A. Şengür, J. Ye, A novel image thresholding algorithm based on neutrosophic similarity score, *Measurement* 58 (2014) 175–186.
- [34] <http://www.mathworks.com/support/sysreq/sv-r2014a/> (accessed 28/6/2015, 05:22 pm).
- [35] <http://www.cs.waikato.ac.nz/ml/weka/documentation.html> (accessed 28/6/2015, 05:22 pm).